ScaleSpaceViz: α-Scale Spaces in Practice¶

F. Kanters, L. Florack, R. Duits, B. Platel, and B. ter Haar Romeny

Eindhoven University of Technology Department of Biomedical Engineering Den Dolech 2, Postbus 513 5600 MB Eindhoven, Netherlands

e-mail: {F.M.W.Kanters, L.M.J.Florack, R.Duits, B.Platel, B.M.terHaarRomeny}@tue.nl

Abstract—Kernels of the so-called α-scale space have the undesirable property of having no closed-form representation in the spatial domain, despite their simple closed-form expression in the Fourier domain. This obstructs spatial convolution or recursive implementation. For this reason an approximation of the 2D α-kernel in the spatial domain is presented using the well-known Gaussian kernel and the Poisson kernel. Experiments show good results, with maximum relative errors of less than 2.4%. The approximation has been successfully implemented in a program for visualizing α-scale spaces. Some examples of practical applications with scale space feature points using the proposed approximation are given.

DOI: 10.1134/S1054661807010129

1. INTRODUCTION

Scale is an essential parameter in computer vision, since it is an immediate consequence of the process of observation, of *measurements*. Observations are always done by *integrating* some physical property with a measurement device—for example, integration (over a spatial area and a time frame)—of reflected light intensity of an object with a CCD sensor in a digital camera or a photoreceptor in our eyes. The range of possibilities of observing certain sizes of objects is bounded on two sides: there is a minimal size, about the size of the smallest aperture, and there is a maximal size, about the size of the whole detector array.

The *front end* of the human visual system (the very first few layers of the visual system) is able to "detect" at different apertures. A good example for this necessity is an image mosaic as shown in Fig. 1. To see the details of each patch we use a small aperture, which prevents us from seeing the global structure. At a large aperture we are able to see the global structure, but not the details of each patch. Objects are only detected at a certain *scale*.

Since one cannot know a priori at which scales objects are present in a scene, it is necessary to detect at multiple scales simultaneously. Scale space theory is the theory of the apertures through which machines and we observe the world. For computer vision systems, the notion of an aperture can be introduced as *blurring* the high-resolution image with a kernel of a certain width. In 1962, Taizo Iijima derived the Gaussian kernel for this purpose from a set of basic axioms in a Japanese paper [1]. Later, papers on linear or Gaussian scale space followed from various other authors, including Witkin [2] and Koenderink [3] in the 1980s. A more recent introduction to scale space can be found in monograph by ter Haar Romeny [4]. It is, however, shown by Duits [5] that, for reasonable axioms, there exists a complete class of kernels leading to the so-called α-scale spaces, of which the Gaussian scale space is a special case ($\alpha = 1$).

Scale space theory makes it possible to look at (spatial) derivatives of the image in a mathematically well-posed way. This is the basis of many well-known feature detectors at the present time, such as blob detectors or edge detectors. It is also shown that the human front-end visual system takes derivatives up to at least fourth order at various scales. It seems that the *differential structure* of an image is important for detecting objects, for human beings as well as for machines.

For a better understanding of image analysis algorithms and the differential structure of images and to explore α-scale spaces, it is important to have a tool that can calculate and visualize these α-scale spaces in

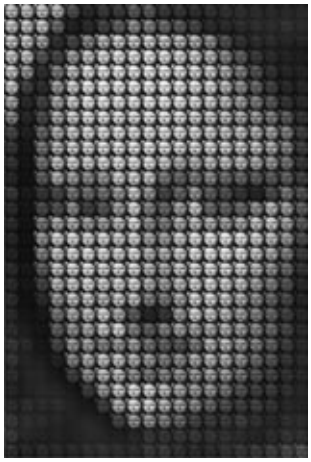

Fig. 1. Image mosaic of the *Mona Lisa*.

¶ The text was submitted by the authors in English.

Received April 13, 2005

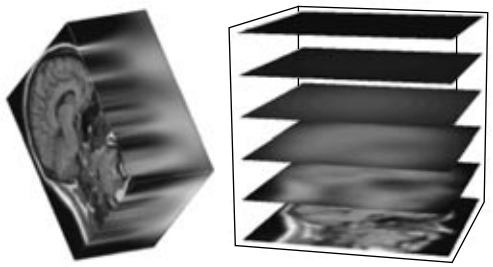

Fig. 2. A scale space of a 2D image as a continuous 3D volume (left) and the same scale space as a stack of sequentially blurred images (right).

an efficient way. Since α kernels are only known in closed form in the Fourier domain, we present a fast and accurate approximation of the kernels in the spatial domain, based on the well-known Gaussian and Poisson kernels. These approximations are implemented in a tool for visualizing α-scale spaces: ScaleSpaceViz.

The remainder of this paper is organized as follows: In Section 2 we will present the general framework of the α scale spaces and the properties of the α-kernels. Next we will present an approximation of these kernels in the spatial domain in Section 3. In Section 4 we present the results of our approximation and compare it with the original kernel. In section 5 we will introduce an application of the approximated kernels. Finally, we provide our conclusions and ideas for future research in Section 6.

2. α-SCALE SPACES

A scale space of an image contains an extra dimension, the *scale*. In a Gaussian scale space the image is blurred according to the evolution process

$$\begin{cases} \dfrac{\partial}{\partial s}u = \Delta u \\ \lim\limits_{s\downarrow 0} u(\cdot, s) = f(\cdot) \text{ in } \mathbb{L}_2(\mathbb{R}^d)\text{-sense,} \end{cases} \tag{1}$$

which leads to convolution of the image with a Gaussian kernel. A scale space of a 2D image is in fact a 3D volume with the scale s as the third axis. In practice, however, a scale space is often seen as a stack of images sequentially blurred by convolution with a kernel. Figure 2 shows an example of a scale space of an image. The α-scale spaces are created using a different evolution process,

$$\begin{cases} \dfrac{\partial}{\partial s}u = -(-\Delta)^{\alpha}u \\ \lim\limits_{s\downarrow 0} u(\cdot, s) = f(\cdot) \text{ in } \mathbb{L}_2(\mathbb{R}^d)\text{-sense} \end{cases} \quad \alpha \in (0, 1], \tag{2}$$

which leads to convolution with a different, so-called α-kernel. Note that for $\alpha = 1$, we indeed obtain the evolution process of the Gaussian scale space. For $\alpha = \frac{1}{2}$ we obtain the evolution process of the Poisson scale space, which has some special properties and can be extended to a monogenic scale space, as described by Felsberg [6]. Figure 3 shows an example of an image blurred with three different α-kernels.

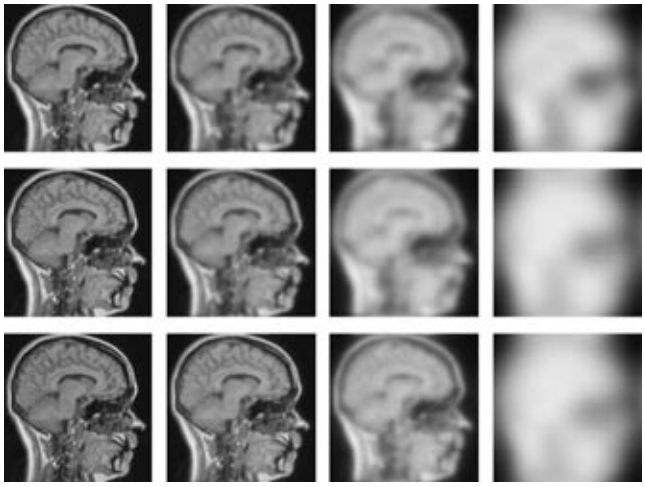

Fig. 3. An example image blurred by different kernels at various scales. Top row: $\alpha = 1$, center row: $\alpha = 3/4$, bottom row: $\alpha = 1/2$.

Recall that the solution of the evolution process in (2) is given by

$$u^{(\alpha)}(\underline{x}, s) = (k_s^{(\alpha)} * f)(\underline{x}), \tag{3}$$

which is called an α-scale space[1], with the α-kernel $k_s^{(\alpha)}: \mathbb{R}^2 \longrightarrow \mathbb{R}$ given in the Fourier domain by

$$\mathcal{F}(k_s^{(\alpha)})(\underline{\omega}_x) = e^{-s\left\|\underline{\omega}_x\right\|^{2\alpha}}, \tag{4}$$

with $0 < \alpha \leq 1$. Note that for $\alpha = 1$ one obtains the well-known Gaussian kernel and for $\alpha = 1/2$ the Poisson kernel. These so-called α-kernels (with $0 < \alpha \leq 1$) are easy to obtain in the Fourier domain, but unfortunately in general there is no closed-form representation in the spatial domain. In the case of a Gaussian or Poisson kernel, one can easily apply an inverse Fourier transform to obtain the kernel in the spatial domain, but in general this is not possible. For a fixed α, however, an expression can be found for the kernel in the spatial domain using the Hankel transform of the kernel in polar coordinates. Using

$$\underline{x} = (r\cos\phi, r\sin\phi), \tag{5}$$

$$\underline{\omega} = (\rho\cos\varphi, \rho\sin\varphi), \tag{6}$$

the kernel in polar coordinates becomes

[1] Also known as α-stable Lévy processes in probability theory.

$$\mathcal{F}(k_s^{(\alpha)})(\underline{\omega}) = e^{-s\rho^{2\alpha}}, \quad \rho = \|\underline{\omega}\|. \tag{7}$$

Any 2D function $f \in \mathbb{L}_2(\mathbb{R}^2)$ in polar coordinates can be decomposed as follows:

$$f(r, \phi) = \sum_{m=0}^{\infty} f_m(r) e^{-im\phi}. \tag{8}$$

The Fourier transform of a product of a radial function with a harmonic function can be written in terms of the Hankel transform [7],

$$\mathcal{F}(f)(\rho, \varphi) = \sum_{m=0}^{\infty} e^{im\varphi} \mathcal{H}_m(f_m)(\rho), \tag{9}$$

with $\mathcal{F}(f)(\rho, \varphi)$ the Fourier transform of f and $\mathcal{H}_m(f_m)(\rho)$ the Hankel transform of f_m defined by

$$\mathcal{H}_m(f)(\rho) = i^m \int_0^{\infty} f(r) r J_m(r\rho) dr, \tag{10}$$

with $J_\nu(z)$ the Bessel function defined by

$$J_\nu(z) = \left(\frac{z}{2}\right)^\nu \sum_{k=0}^{\infty} \frac{-1^k}{k!\Gamma(k+\nu+1)} \left(\frac{z}{2}\right)^{2k}. \tag{11}$$

Since our kernel is independent of φ, we have

$$(\mathcal{H}_0(r \mapsto k_s^{(\alpha)}(\underline{x})))(\rho) = \mathcal{F}(k_s^{(\alpha)})(\underline{\omega}) = e^{-s\rho^{2\alpha}}. \tag{12}$$

The Hankel transformation equals its inverse transformation (for functions independent of ϕ); hence, the inverse Fourier transform of our kernel becomes the Hankel transform of the kernel in the Fourier domain:

$$\begin{gathered} k_s^{(\alpha)}(r) = \mathcal{H}_0[\rho \mapsto (\mathcal{F}(k_s^{(\alpha)}))(\underline{\omega})](r), \\ r = \|\underline{x}\|, \quad \rho = \|\underline{\omega}\|. \end{gathered} \tag{13}$$

Using the Hankel transformation, it is possible to obtain an expression for the α-kernel in the spatial domain for a fixed α only. For some values of α, the expression can become quite complicated, involving hypergeometric functions. Therefore, an approximation of the α-kernel in the spatial domain is presented.

3. APPROXIMATION OF THE α-KERNEL IN THE SPATIAL DOMAIN

An approximation of the α-kernel is proposed using a linear combination of one Gaussian kernel and one Poisson kernel. In the Fourier domain, the approximation becomes

$$e^{-s\|\omega\|^{2\alpha}} \approx a(\alpha) e^{-s_g(\alpha)\|\omega\|^2} + b(\alpha) e^{-s_p(\alpha)\|\omega\|}. \tag{14}$$

Note that a, b, s_g (Gauss scale), and s_p (Poisson scale) are constants, which may depend on α. In order to obtain a correct amplitude for $\omega = 0$, we must have $a + b = 1$, which results in

$$e^{-s\|\omega\|^{2\alpha}} \approx a(\alpha) e^{-s_g(\alpha)\|\omega\|^2} + (1 - a(\alpha)) e^{-s_p(\alpha)\|\omega\|}. \tag{15}$$

An exact result is desired for $\alpha = 1$ and $\alpha = 1/2$, which results in the following constraints:

$$\begin{gathered} a(1) = 1, \quad s_g(1) = s \\ a(1/2) = 0, \quad s_p(1/2) = s. \end{gathered} \tag{16}$$

For dimensionality reasons and using these constraints, it is natural to assume

$$\begin{gathered} s = t^\alpha, \text{ and } s_g = c_1(\alpha) t, \\ \text{and } s_p = c_2(\alpha)\sqrt{t} \end{gathered} \tag{17}$$

with constraints

$$c_1(1) = 1 \text{ and } c_2(1/2) = 1, \tag{18}$$

which results in

$$\begin{gathered} s_g(\alpha) = c_1(\alpha) t = c_1(\alpha) s^{\frac{1}{\alpha}} \\ s_p(\alpha) = c_2(\alpha)\sqrt{t} = c_2(\alpha) s^{\frac{1}{2\alpha}}. \end{gathered} \tag{19}$$

Using the dimensionless frequency $\|\sqrt{t}\,\omega\| = \rho$, Eq. (15) can be rewritten as

$$e^{-\rho^{2\alpha}} \approx a(\alpha) e^{-c_1(\alpha)\rho^2} + (1 - a(\alpha)) e^{-c_2(\alpha)\rho}. \tag{20}$$

Note that for all relevant frequencies we can assume (roughly) that $\rho \le 1$. Using a Taylor expansion up to order N around $\rho = 0$, we obtain

$$\begin{aligned} \sum_{n=0}^{N} (-1)^n \frac{\rho^{2\alpha n}}{n!} &\approx a(\alpha) \sum_{n=0}^{N} (-1)^n \frac{c_1^n \rho^{2n}}{n!} \\ &+ (1 - a(\alpha)) \sum_{n=0}^{N} (-1)^n \frac{c_2^n \rho^n}{n!}. \end{aligned} \tag{21}$$

To obtain an expression for $a(\alpha)$, (21) may be integrated over all *relevant* frequencies:

$$\begin{aligned} &\int_0^1 \left(\sum_{n=0}^{N} (-1)^n \frac{\rho^{2\alpha n}}{n!} \right) d\rho \\ &\approx \int_0^1 a(\alpha) \sum_{n=0}^{N} (-1)^n \frac{c_1^n \rho^{2n}}{n!} \\ &+ (1 - a(\alpha)) \sum_{n=0}^{N} (-1)^n \frac{c_2^n \rho^n}{n!} d\rho. \end{aligned} \tag{22}$$

The left-hand side of this equation is a function only depending on α, while the right-hand side only depends on a, c_1, and c_2. For a first-order Taylor expansion ($N = 1$), the solution of $a(\alpha)$ in (22) can be expressed in α, c_1, and c_2:

$$a(\alpha) = \frac{3(-2 + (1 + 2\alpha)c_2)}{(1 + 2\alpha)(-2c_1 + 3c_2)}. \quad (23)$$

To find an expression for $c_1(\alpha)$ and $c_2(\alpha)$, the amplitude of the α-kernel in the spatial domain at the origin is calculated using the Hankel transform (13):

$$k_s^{(\alpha)}(0) = \mathcal{H}_0[\rho \mapsto (\mathcal{F}(k_s^{(\alpha)}))(\omega)](0) = \frac{\Gamma\left(1 + \frac{1}{\alpha}\right)}{4\pi s^{\frac{1}{\alpha}}}. \quad (24)$$

The amplitudes at the origin for the Gaussian and Poisson kernel in two dimensions are given by

$$G(0) = \frac{1}{4\pi s_g} \quad (25)$$

and

$$P(0) = \frac{1}{2\pi s_p^2}. \quad (26)$$

Combined with (24) this results in the equation

$$\frac{\Gamma\left(1 + \frac{1}{\alpha}\right)}{4\pi s^{\frac{1}{\alpha}}} = \frac{a(\alpha)}{4\pi c_1(\alpha) s^{\frac{1}{\alpha}}} + \frac{1 - a(\alpha)}{2\pi c_2^2 s^{\frac{1}{\alpha}}}. \quad (27)$$

In order to solve this equation for c_1 and c_2, an extra equation is needed. If $c_2^2 = 2c_1$ is chosen as an extra constraint, the amplitude for the α-kernel at origin is not dependent on $a(\alpha)$ and we may readily solve for c_1 and, thus, c_2:

$$c_1(\alpha) = \frac{1}{\Gamma\left(1 + \frac{1}{\alpha}\right)}, \qquad c_2(\alpha) = \sqrt{\frac{2}{\Gamma\left(1 + \frac{1}{\alpha}\right)}}. \quad (28)$$

Note that now the unknown parameters $a(\alpha)$, $b(\alpha)$, $s_g(\alpha)$, and $s_p(\alpha)$ of (14) are expressed in terms of α while obeying the constraints of (16) and (18).

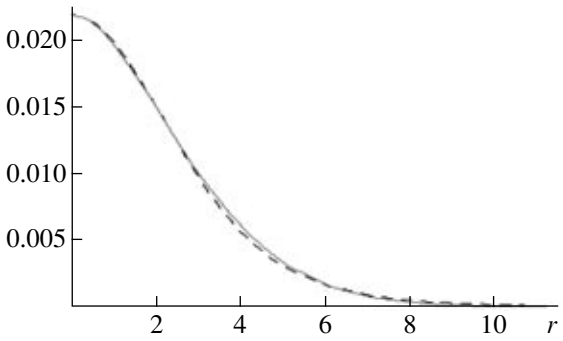

Fig. 4. 1D cross section of the α-kernel (solid) and the approximated kernel (dashed) in the spatial domain for α = 7.5 and $s = 3$.

4. RESULTS

The approximation presented in the previous section still contains a rather complicated Gamma function. Since $1/2 \le \alpha \le 1$, only a small, very smooth part of the Gamma function is actually used in our expressions. With a program like Mathematica [8], a good numerical approximation can be found for this part of the Gamma function. Experiments were conducted using the following numerical approximations for $c_1(\alpha)$, $c_2(\alpha)$, and $a(\alpha)$:

$$c_1(\alpha) = \frac{-1.5374 + 5.0722\alpha}{1 + 1.4548\alpha + 1.0800\alpha^2}$$

$$c_2(\alpha) = \sqrt{\frac{-3.0748 + 10.1444\alpha}{1 + 1.4548\alpha + 1.0800\alpha^2}} \quad (29)$$

$$a(\alpha) = \frac{3(-2 + (1 + 2\alpha)c_2)}{(1 + 2\alpha)(-2c_1 + 3c_2)}.$$

Using (15) and (29), simple approximations of the α-kernel in the spatial domain can be made. Figure 4 shows the 1D cross section of the α-kernel and the approximation for $\alpha = 0.75$ and $s = 3$.

The approximation is of course exact for $r = 0$ (due to constraints) and for $r = \infty$. The maximum error between the α-kernel and the approximated kernel can be defined as

$$\text{Maximum relative error} = \frac{\left\| k_s^{(\alpha)} - g_s^{(\alpha)} \right\|_\infty}{\left\| k_s^{(\alpha)} \right\|_\infty}, \quad (30)$$

with $k_s^{(\alpha)}$ being the α-kernel and $g_s^{(\alpha)}$ the approximated kernel. Figure 5 shows the maximum relative error between the α-kernel and the proposed approximation for various α and s.

Note that the maximum relative error should be independent of scale, which is also found experimentally. The worst maximum relative error, 2.36%, is found approximately at $\alpha = 0.65$.

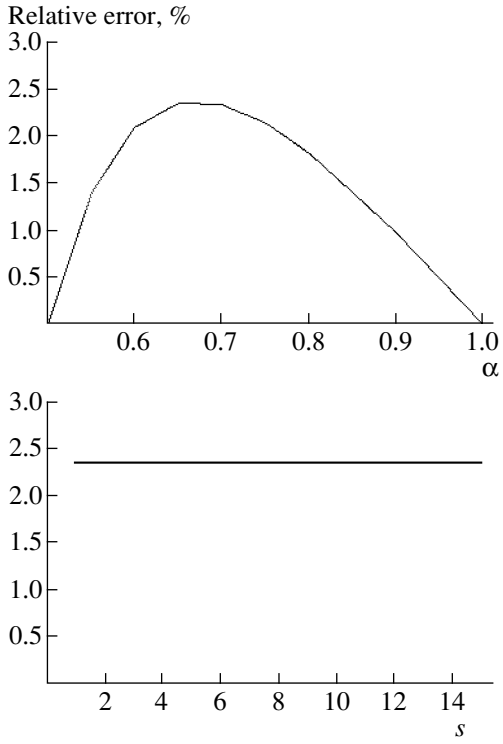

Fig. 5. Maximum relative error between α-kernel and approximation for various α with scale fixed at $s = 3$ (top) and for various s with fixed at $\alpha = 0.7$ (bottom).

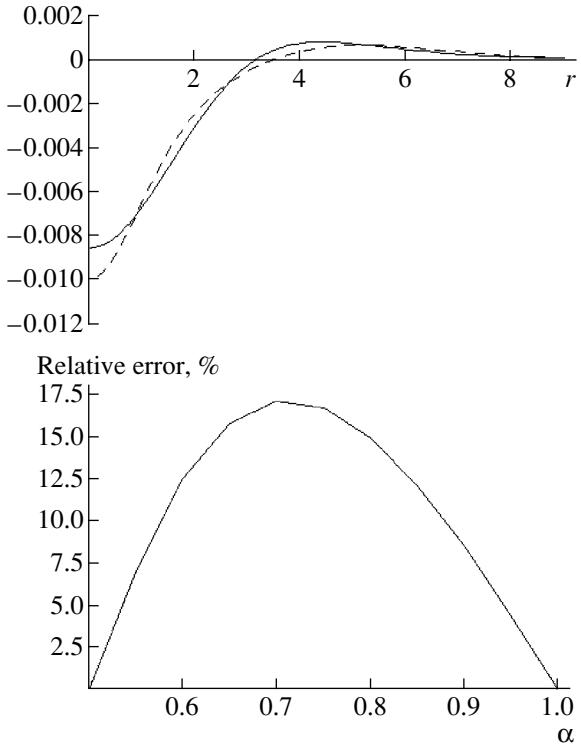

Fig. 6. Top: example of the Laplacian of the α-kernel (solid line) and the Laplacian of the approximated kernel (dashed line) for the zeroth order optimization. Bottom: maximum relative error between the Laplacian of the α-kernel and approximation for various α with scale fixed at $s = 3$.

4.1. Spatial Derivatives

In order to obtain derivatives of an image at a certain scale, one can carry out a convolution of the image with a derivative of the kernel. In this section we show how our approximation of the α-kernel performs if derivatives are taken. For simplicity, we will only show the results for the Laplacian. The Laplacian in polar coordinates is defined by

$$\mathcal{L}(r, \phi) = \frac{\partial^2 f}{\partial r^2} + \frac{1}{r}\frac{\partial f}{\partial r} + \frac{1}{r^2}\frac{\partial^2 f}{\partial \phi^2}, \tag{31}$$

which can be simplified, because our kernel is only dependent on r:

$$\mathcal{L}(r) = \frac{\partial^2 f}{\partial r^2} + \frac{1}{r}\frac{\partial f}{\partial r}. \tag{32}$$

Using (32) on (15), one can find an approximation of the Laplacian kernel. However, the parameters are still optimized for the zeroth-order kernel; hence, the error will be too large. Figure 6 shows the resulting Laplacian kernel and the maximum relative error for the zeroth-order optimization. To improve the approximation of the Laplacian kernel, the steps of Eq. (24) up to (36) are repeated for the Laplacian kernel. First, the amplitude of the kernel at the origin is again calculated:

$$k_s^{(\alpha)}(0) = \mathcal{H}_0[\rho \mapsto (\mathcal{F}(-\omega^2 k_s^{(\alpha)}))(\underline{\omega})](0) = -\frac{\Gamma\left(1 + \frac{2}{\alpha}\right)}{8\pi s^{\frac{2}{\alpha}}}. \tag{33}$$

The amplitude at the origin for the approximated kernel in two dimensions is given by

$$\hat{k}_s^{(\alpha)}(0) = \frac{-\frac{a}{c_1^2} + \frac{12(a-1)}{c_2^4}}{4\pi s^{\frac{2}{\alpha}}}. \tag{34}$$

Combined with (33) this results in the equation

$$-\frac{\Gamma\left(1 + \frac{2}{\alpha}\right)}{8\pi s^{\frac{2}{\alpha}}} = \frac{-\frac{a}{c_1^2} + \frac{12(a-1)}{c_2^4}}{4\pi s^{\frac{2}{\alpha}}}. \tag{35}$$

If $c_2^4 = 12c_1^2$ is chosen as an extra constraint, the amplitude for the α-kernel at the origin is not depen-

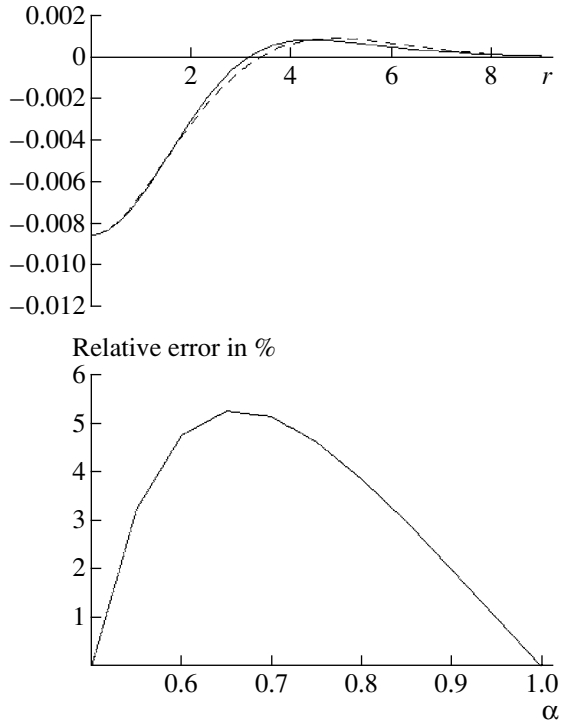

Fig. 7. Top: example of the Laplacian of the α-kernel (solid line) and the Laplacian of the approximated kernel (dashed line) optimized for the Laplacian. Bottom: maximum relative error between the Laplacian of the α-kernel and approximation for various α with scale fixed at $s = 3$.

dent on $a(\alpha)$ and we may readily solve for c_1 and, thus, c_2:

$$c_1(\alpha) = \sqrt{\frac{2}{\Gamma\left(1+\frac{2}{\alpha}\right)}}$$
$$c_2(\alpha) = \sqrt[4]{\frac{24}{\Gamma\left(1+\frac{2}{\alpha}\right)}}. \quad (36)$$

Figure 7 shows the resulting kernel with the parameters optimized for the Laplacian kernel and the maximum relative error. Note that the results are, indeed, much improved. In a similar fashion, the parameters can be optimized for other derivatives of the kernel.

5. IMPLEMENTATION AND EXAMPLES

The presented approximation is implemented in a software package by the name of ScaleSpaceViz [9]. It is mainly designed for research purposes, to learn more about α-scale spaces and the *deep structure* of images [3].

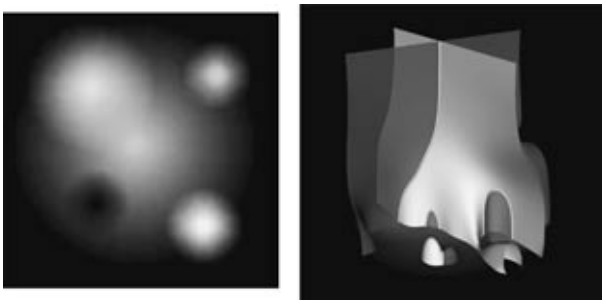

Fig. 8. Left: simple 2D image with some Gaussian blobs. Right: zero crossings of x- and y-derivative surfaces (z axis is scale) and their intersections (critical paths).

5.1. Interest Points

The program can calculate and visualize special interest points in scale space by calculating zerocrossings of 3D volumes. Consider, for example, the spatial critical points defined by

Definition 1. Spatial critical points are points where the spatial gradient is zero. For 2D images these points are maxima, minima, or saddles.

If these points are tracked through scale, so called critical paths are obtained. These paths are the intersections of the zerocrossings of the x- and y-derivative of the scale space of a 2D image. Figure 8 shows the critical paths of a simple blob image plus the zerocrossing surfaces of the x- and y-derivative.

In the diffusion process, extrema can merge with saddles or extrema-saddle pairs can be created. This happens at the so-called top points, which are defined by

Definition 2. Top points are spatial critical points where the Hessian degenerates ($\det H = 0$). For generic 2D images, these points are annihilations or creations of saddles with maxima or minima,

where the Hessian of a 2D image f is given by

$$H(f) = \nabla\nabla f = \begin{pmatrix} \partial_x^2 f & \partial_x\partial_y f \\ \partial_y\partial_x f & \partial_y^2 f \end{pmatrix}. \quad (37)$$

These points are the intersections of the zerocrossings of the determinant of the Hessian with the critical paths. Other points of interest are, for example, scale space saddles, which are also spatial critical points, but also have a zero scale derivative (which by definition equals a zero Laplacian in a Gaussian scale space). These points are intersections of the zerocrossings of the Laplacian with the critical paths. Figure 9 shows again the simple blob image, with the critical paths, top points, and scale space saddles. In Fig. 10 some exam-

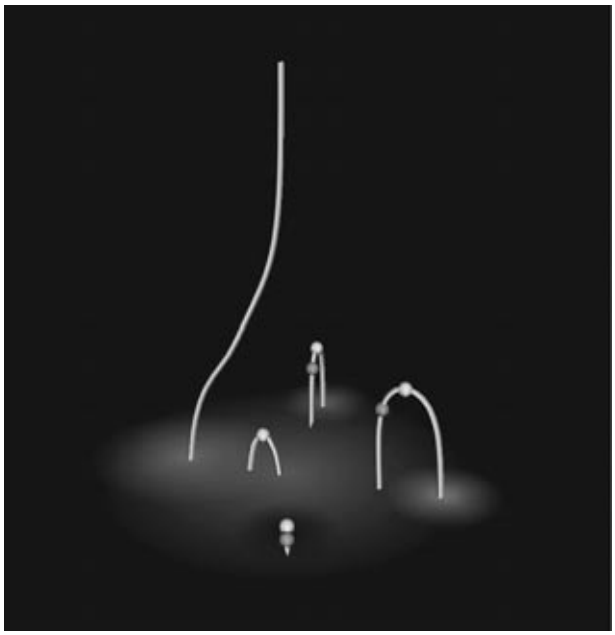

Fig. 9. Critical paths of the blob image from Fig. 8. The light dots show the top points and the dark dots show the scale space saddles. Note that not all paths have scale space saddles and that there can be more saddles on one critical path. There is, however, *at least* one top point in each critical path (with the remaining path having a top point in infinity).

ples of critical paths and top points with creation–annihilation pairs are shown.

5.2. Approximated α-Scale Space Kernel

Critical paths and top points can be calculated for any (α) scale space, this is not limited to the Gaussian scale space. The paths of different α-scale spaces will not be the same for an image, and even topological differences will occur. Figure 11 shows the critical paths and top points of an image for three different α's. To confirm the quality of the approximated kernels as described previously, the program can calculate critical paths and top points for α-scale spaces both using convolution in the spatial domain and multiplication in the Fourier domain. Figure 12 shows the critical paths and top points of an image using the Fourier and the spatial convolution methods.

5.3. Stability of Scale Space Interest Points

For any practical application of scale space interest points, it is crucial to have information about the stability of those points under small perturbations. For example, critical points depend on the position of maxima, minima, and saddles in the image. In almost homogeneous areas in the image, the extrema merely depend on noise. These points will thus be very unstable under small perturbations and not very useful for applications. Figure 13 shows the critical paths and top points of different noise realizations of an image. Note that there is indeed a difference between stable top points in regions with much structure and unstable top points in

Fig. 10. Examples of creation–annihilation pairs of extrema and saddles. Top and center: two artificial test images with dumbbell examples. Bottom: part of an MR brain image with creation–annihilation pairs.

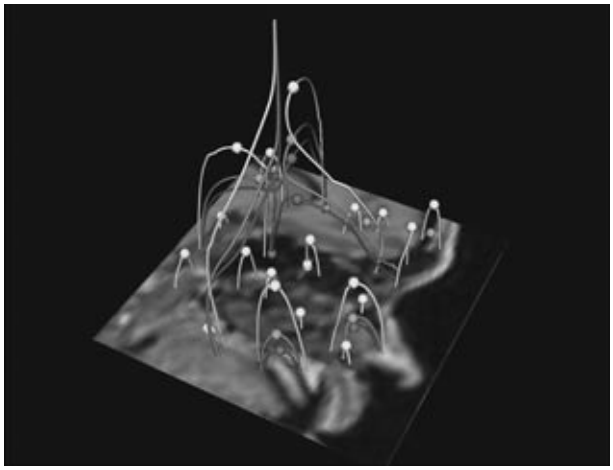

Fig. 11. Critical paths from scale spaces of an MR image with $\alpha = 0.5$ (white), $\alpha = 0.75$ (light gray) and with $\alpha = 1.0$ (dark gray). Note that there are topological differences in the large paths in the center between the different α-scale spaces.

regions with little structure. Platel et al. presented a stability measure for top points based on the total variation norm [10], which could also be used for other critical points. Balmachnova et al. presented a more elaborate stability measure for top points that also takes directions into account [11].

5.4. Applications Using Scale Space Interest Points

Multiscale interest points can potentially be used in several applications. Nielsen and Lillholm compared the descriptive power of different scale space interest points [12] by means of reconstruction. They look at the metameric class of images that have the same interest points. More recent results of reconstructions from top points based on a new reconstruction scheme can be found in the authors' work [13, 14]. Figure 14 shows an example of reconstructions from 19 and 63 top points of an image, respectively. The ordering is according to the stability measure, as described previously.

Scale space interest points have also been proven useful in matching applications. For example, Lowe [15] used blob points for finding objects in a cluttered scene. Platel et al. [16] used top points to match faces in a database. From each image the top points are extracted and a directed acyclic graph (DAG) is created using scale space tessellation. Two images are compared by embedding the DAGs into a high dimensional vector space and calculating the Earth Movers Distance [17] between the two embedded DAGs (See Fig. 15).

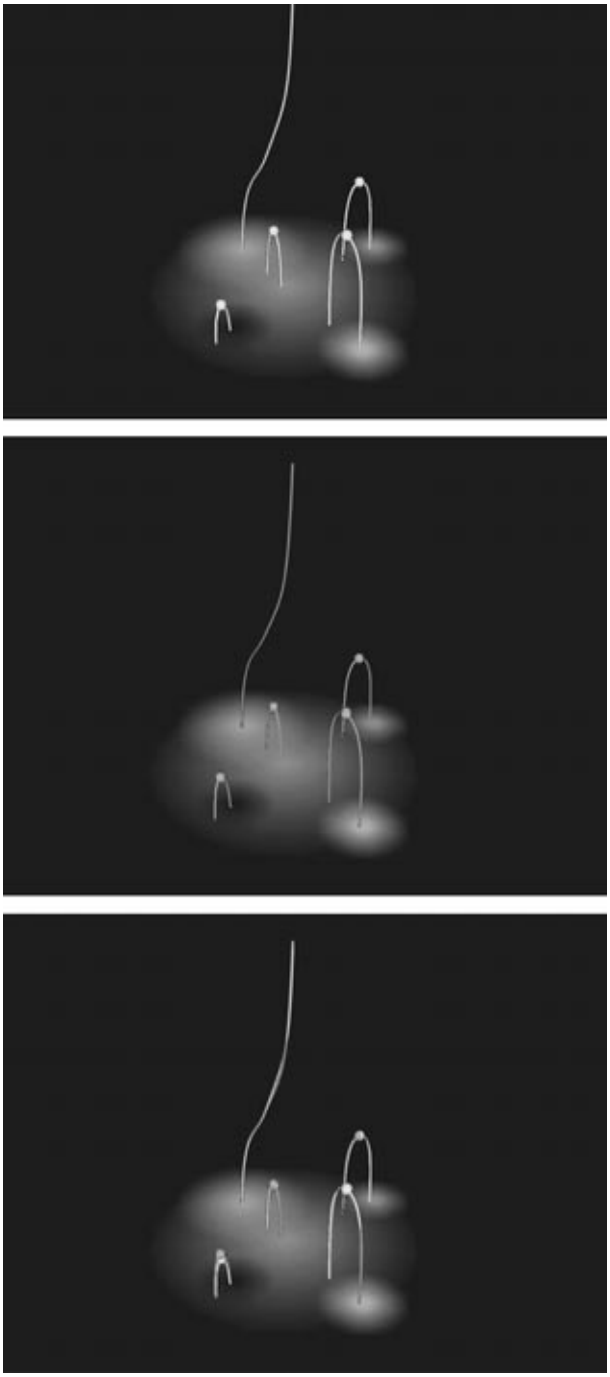

Fig. 12. Experiments to confirm the approximation of the α-kernel in the spatial domain. Top: scale space calculated in the Fourier domain with the original kernel ($\alpha = 0.75$). Center: the same scale space calculated with the approximated kernel in the spatial domain. Bottom: the two methods projected on top of each other; the Fourier method in white, the convolution method in gray.

6. CONCLUSIONS AND FUTURE RESEARCH

Using α-scale spaces in practice can be a problem, since the corresponding kernels are only known in closed form in the Fourier domain for $1/2 < \alpha < 1$. Some applications, however, can make advantage of a spatial representation of an α-kernel. We solve this problem by approximating a 2D α-kernel in the spatial

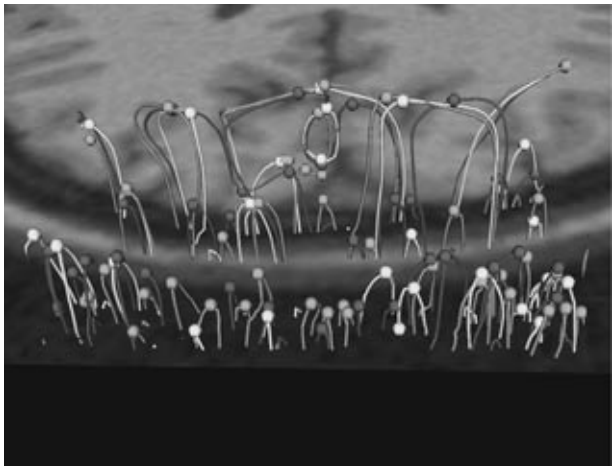

Fig. 13. Critical paths and top points of three different noise realizations of a CT brain image (in white, light gray, and dark gray). Note that there is no clear relation between the position of top points of the three noise realizations in the dark image area at the bottom; in this almost homogeneous part of the image, the critical paths and the top points are dominated by noise and are thus unstable. In areas with more structure (top part), one can see a clear relationship between the critical paths and top points of the different noise realizations. The top points are very stable *perpendicular* to the elongated structure and less stable *along* the elongated structure. Note that the critical paths can be very different in stable areas, while the positions of the top points are almost the same.

domain with a linear combination of one Gaussian kernel and one Poisson kernel. The maximum relative error between the α-kernel and the approximation is low (less than 2.4%) and independent of scale. With the presented parameters, the error propagates in the derivatives of the kernel, resulting in a maximum relative error of approximately 12% for a second-order derivative of the kernel. This is solved by adding constraints for derivatives to calculate the parameters in a similar way as we have done for the zeroth-order case.

Fig. 14. Image reconstruction from top points. Left: original image of Lena's eye (64×64 pixels). Center: reconstruction from 19 top points with up to fourth-order derivatives in each top point. Right: reconstruction from 63 top points with up to fourth-order derivatives in each top point. Adapted from [13].

The presented approximation is implemented in the software tool ScaleSpaceViz. This tool has proven to be useful in exploring the deep structure of images and constructing applications involving scale space interest points, such as reconstruction and matching.

Future research will include extensions of the previously mentioned applications. Using reconstruction from scale space interest points, one can perform image editing by applying an operation on the interest points and making a reconstruction, for example, removing parts in a scene by removing the corresponding interest points or morphing one image into the other by moving the interest points from one set to the other. Combined with matching algorithms, reconstruction can result in removing a particular object from a scene automati-

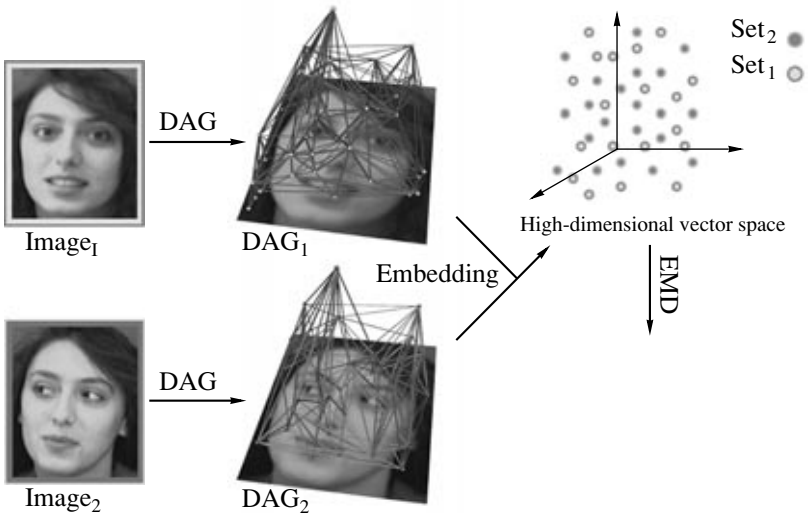

Fig. 15. Image matching using top points. To compare two images from a database (e.g., a query image and a candidate from an image database) one calculates the top points of both images. A directed acyclic graph (DAG) is created for each image using some proper distance measure. These DAGs are embedded in a metric space and using the EMD a distance between the two images is calculated. Adapted from [16].

cally. It is also possible to follow the movement of interest points in an image sequence to extract motion paths of objects.

ACKNOWLEDGMENTS

This work is part of the DSSCV project supported by the IST Programme of the European Union, IST-2001-35443.

REFERENCES

1. T. Iijima, "Basic Theory on Normalization of a Pattern (In Case of Typical One-Dimensional Pattern)," Bulletin of Electrical Laboratory **26**, 368–388 (1962).
2. A. P. Witkin, "Scale-space filtering," in *Proceedings of the International Joint Conference on Artificial Intelligence, Karlsruhe, Germany, 1983*, pp. 1019–1022.
3. J. J. Koenderink, "The Structure of Images," Biological Cybernetics **50**, 363–370 (1984).
4. B. M. ter Haar Romeny, *Front-End Vision and Multistage Image Analysis* (Kluwer Academic Publishers, 2002).
5. R. Duits, M. Felsberg, L. Florack, and B. Platel, "α-Scale Spaces on a Bounded Domain," in *Proceedings of Scale Space Methods in Computer Vision, 4th International Conference, Scale Space 2003, Isle of Skye, UK, June 2003,* Ed. by L. Griffin and M. Lillholm (Springer), pp. 494–510.
6. M. Felsberg, R. Duits, and L. M. J. Florack, "The Monogenic Scale Space on a Bounded Domain and Its Applications," in *Proceeding of Scale Space Methods in Computer Vision, 4th International Conference, Scale Space 2003*, *Isle of Skye, UK, June 2003,* Ed. by L. Griffin and M. Lillholm (Springer), pp. 209–224.
7. L. Faraut and K. Harzallah, *Deux Cours d'Analyse Harmonique—Ecole d'Ete d'Analyse Harmonique de Tunis* (Birkhaeuser, Basel, 1987).
8. S. Wolfram, *Mathematica: A System for Doing Mathematics by Computer,* 2nd ed. (Addison-Wesley, 1991).
9. www.bmi2.bmt.tue.nl/image-analysis/people/fkanters (ScaleSpaceViz: Software for visualizing α-scale spaces, 2004).
10. B. Platel, F. M. W. Kanters, L. M. J. Florack, and E. G. Balmachnova, "Using Multiscale Top Points in Image Matching," in *Proceedings of the 11th International Conference on Image Processing* (Singapore, October, 2004).
11. E. G. Balmachnova, L. M. J. Florack, B. Platel, F. M. W. Kanters, and B. M. ter Haar Romeny, "Stability of Top Points in Scale Space," in *Proceedings of the 5th International Conference on Scale Space and PDE Methods in Computer Vision, Hofgeismar, Germany, April 7–9 2005*, Eds. by N. Sochen, R. Kimmel, and J. Weickert, (Springer, 2005), Vol. LNCS3459, pp. 62–72.
12. M. Nielsen and M. Lillholm, "What do Features Tell About Images?," in *Scale-Space and Morphology in Computer Vision*, in *Proceedings of the Third International Conference, Scale-Space 2001, Vancouver, Canada,* Ed. by M. Kerckhove, (Springer, Berlin, July 2001), Vol. LNCS2106, pp. 39–50.
13. F. M. W. Kanters, M. Lillholm, R. Duits, B. J. Janssen, B. Platel, and L. M. J. Florack, "On Image Reconstruction from Multiscale Top Points," in *Proceedings of the 5th International Conference on Scale Space and PDE Methods in Computer Vision, Hofgeismar, Germany, April 7–9 2005*, Eds. by N. Sochen, R. Kimmel, and J. Weickert (Springer, 2005), Vol. LNCS3459, pp. 431–442.
14. B. J. Janssen, F. M. W. Kanters, R. Duits, and L. M. J. Florack, "A Linear Image reconstruction Framework Based on Sobolev Type Inner Products," in *Proceedings of the 5th International Conference on Scale Space and PDE Methods in Computer Vision, Hofgeismar, Germany, April 7–9 2005*, Eds. by N. Sochen, R. Kimmel, and J. Weickert, Eds., (Springer, 2005), Vol. LNCS3459.
15. D. G. Lowe, "Object Recognition from Local Scale-Invariant Features," in *Proceedings of the International Conference on Computer Vision ICCV, Corfu, 1999*, pp. 1150–1157.
16. B. Platel, M. Fatih Demirci, A. Shokoufandeh, L. M. J. Florack, F. M. W. Kanters, and S. J. Dickinson, "Discrete Representation of Top Points Via Scale Space Tessellation," in *Proceedings of the 5th International Conference on Scale Space and PDE Methods in Computer Vision, Hofgeismar, Germany, April 7–9 2005,* Eds. by N. Sochen, R. Kimmel, and J. Weickert (Springer, 2005), Vol. LNCS3459, pp. 73–84.
17. L. J. Guibas, Y. Rubner, and C. Tomasi, "A Metric for Distributions with Applications to Image Databases," in *Proceedings of IEEE International Conference on Computer Vision, Bombay, India, 1998*, pp. 59–66.

Frans Kanters received his MSc degree in Electrical Engineering in 2002 from the Eindhoven University of Technology in the Netherlands. Currently he is working on his PhD at the Biomedical Imaging and Informatics group at the Eindhoven University of Technology. His PhD work is part of the "Deep Structure, Singularities, and Computer Vision (DSSCV)" project sponsored by the European Union. His research interests include scale space theory, image reconstruction, image processing algorithms, and hardware implementations thereof.

Luc Florack received his MSc degree in theoretical physics in 1989 and his PhD degree cum laude in 1993 with a thesis on image structure, both from Utrecht University, the Netherlands. During the period from 1994 to 1995, he was an ERCIM/HCM research fellow at INRIA Sophia-Antipolis, France, and IN-ESC Aveiro, Portugal. In 1996 he was an assistant research professor at DIKU, Copenhagen, Denmark, on a grant from the Danish Research Council. From 1997 to June 2001, he was an assistant research professor at Utrecht University in the Department of Mathematics and Computer Science. Since June 1, 2001, he has been working as an assistant professor and, then, as an associate professor at Eindhoven University of Technology, Department of Biomedical Engineering. His interest includes all multiscale structural aspects of signals, images, and movies and their applications to imaging and vision.

Remco Duits received his MSc degree (cum laude) in Mathematics in 2001 from the Eindhoven University of Technology, the Netherlands. Today he is a PhD student at the Department of Biomedical Engineering at the Eindhoven University of Technology on the subject of multiscale perceptual organization. His interest subtends functional analysis, group theory, partial differential equations, multiscale representations and their applications to biomedical imaging and vision, perceptual grouping. Currently, he is finishing his thesis "Perceptual Organization in Image Analysis (A Mathematical Approach Based on Scale, Orientation and Curvature)." During his PhD work, several of his submissions at conferences were chosen as selected or best papers—in particular, at the PRIA 2004 conference on pattern recognition and image analysis in St. Petersburg, where he received a best paper award (second place) for his work on invertible orientation scores.

Bram Platel received his Masters Degree cum laude in biomedical engineering from the Eindhoven University of Technology in 2002. His research interests include image matching, scale space theory, catastrophe theory, and image-describing graph constructions. Currently he is working on his PhD in the Biomedical Imaging and Informatics group at the Eindhoven University of Technology.

Bart M. ter Haar Romany is full professor in Biomedical Image Analysis at the Department of Biomedical Engineering at Eindhoven University of Technology. He has been in this position since 2001. He received a MSc in Applied Physics from Delft University of Technology in 1978, and a PhD on neuromuscular nonlinearities from Utrecht University in 1983. After being the principal physicist of the Utrecht University Hospital Radiology Department, in 1989 he joined the department of Medical Imaging at Utrecht University as an associate professor. His interests are mathematical aspects of visual perception, in particular linear and non-linear scale-space theory, computer vision applications, and all aspects of medical imaging. He is author of numerous papers and book chapters on these issues; he edited a book on non-linear diffusion theory and is author of an interactive tutorial book on scale-space theory in computer vision. He has initiated a number of international collaborations on these subjects. He is an active teacher in international courses, a senior member of IEEE, and IEEE Chapter Tutorial Speaker. He is chairman of the Dutch Biophysical Society.